Journal of Environmental Chemical Engineering 13 (2025) 119270

Contents lists available at ScienceDirect

Journal of Environmental Chemical Engineering

journal homepage: www.elsevier.com/locate/jece

Adsorption and recovery of the fumigant sulfuryl fluoride from air

Philip S. Pein [a,*,1], Carsten Zetzl [a,2], Irina Smirnova [a,b,3]

[a] Hamburg University of Technology, Institute of Thermal Separation Processes, Eissendorfer Str. 38, Hamburg 21073, Germany
[b] United Nations University Hub on Engineering to Face Climate Change at the Hamburg University of Technology, United Nations University Institute for Water, Environment and Health (UNU-INWEH), Hamburg, Germany

ARTICLE INFO

Keywords:
Activated carbon
Adsorption
Fumigant
Recovery
Sulfuryl Fluoride
HiSiv 3000
Zeolite

ABSTRACT

Global emissions of the fumigant and greenhouse gas sulfuryl fluoride (SO_2F_2) are rising, partly due to its unfiltered venting to the atmosphere after fumigation. Although European law demands emission control for SO_2F_2, this currently has little practical consequence, due to a lack of feasible separation methods for SO_2F_2 from air. An evaluation of the state-of-the-art shows that gas adsorption has a high potential to be practically implemented to mitigate SO_2F_2 emissions from fumigation. In a screening of different commercial adsorbents, the activated carbon Air CC 816 and the zeolite HiSiv 3000 indicated promising adsorption capacities for SO_2F_2, in dry and humid air. Thereby, this study presents the first comprehensive screening of commercial adsorbents for SO_2F_2 recovery in general and the first report on SO_2F_2 adsorption on activated carbons and zeolites under humid conditions. Air CC 816 and HiSiv 3000 appear to primarily adsorb SO_2F_2 physically, allowing a recovery for possible reuse and omitting catalytic decomposition of SO_2F_2. For the zeolite HiSiv 3000, SO_2F_2 isotherms and mass transfer kinetics are measured and used to derive the adsorption enthalpy. On this zeolite, water and SO_2F_2 exhibit co-adsorption behaviour where water displaces SO_2F_2. Based on experimental characterization, a concept for an adsorptive recovery on HiSiv 3000 is designed, suggesting the suitability of hot gas desorption with additional external heat input, or steam desorption, for SO_2F_2 recovery. Finally, a first field test for SO_2F_2 adsorption after container fumigation already showed promising breakthrough times on HiSiv 3000.

1. Introduction

The insecticide sulphuryl fluoride (SO_2F_2) was introduced in 1956 as a fumigant [1] and has been used since in post-harvest pest control, structural fumigation, and the treatment of export containers for various goods, where some countries' import regulations demand its application [2,3]. Its global use as a fumigant increased since 2005, when it was introduced as a supposedly more environmentally friendly alternative to methyl bromide [4], which was phased out for fumigation applications, due to its ozone-depleting properties recognized in the Montreal Protocol 1989 [5–7]. In parallel, the global amount of SO_2F_2 in the atmosphere more than doubled from 2004 to 2022 [6]. Meanwhile, several studies indicate that SO_2F_2 is a potent greenhouse gas with a global warming potential (GWP) of 4780 ± 1434 CO_2 equivalents [8].

Since March 11, 2024, the EU regulation (EU) 2024/573 on fluorinated greenhouse gases explicitly demands the capture of SO_2F_2 after fumigation if technically and economically feasible [9]. In Germany, also the regulation "Technische Anleitung zur Reinhaltung der Luft" (TA-Luft), an implementation of the German Federal Emission Control Act ("Bundes-Immissionsschutzgesetz"), demands the separation of SO_2F_2 from the off-gas for the approval of new fumigation systems since December 2021, according to TA-Luft, No.5.4.10.22.1 [10]. Corresponding technologies are to be retrofitted to existing equipment by December 2026 [10]. With the current state of the art, however, SO_2F_2 removal from fumigation off-gas is not economical.

During the fumigation of a structure or container, SO_2F_2 is flashed from a pressure vessel and fed as vapour into the partially sealed object [11]. Depending on the required dosage, this results in a gas mixture with a loading of up to 105 g m^{-3} SO_2F_2 (approx. 2.5 vol% under typical fumigation conditions) [12]. As there are currently no established containment methods for SO_2F_2, the fumigation off-gas is usually emitted directly into the atmosphere after a single use by venting,

* Corresponding author.
E-mail address: philip.sidney.pein@tuhh.de (P.S. Pein).
[1] ORCID: 0009-0007-8092-3575
[2] ORCID: 0000-0002-2241-906X
[3] ORCID: 0000-0003-4503-4039

https://doi.org/10.1016/j.jece.2025.119270
Received 26 July 2025; Received in revised form 5 September 2025; Accepted 12 September 2025
Available online 13 September 2025

leading to the emission of the total remaining SO_2F_2. Depending on the fumigated object's sealing quality, a considerable amount of SO_2F_2 can be emitted through leakage already during the treatment time [13–15], with typical half loss times of 20 h for buildings [11,14]. While this limits the potential of emission mitigation, it is essential to develop economical treatment methods for fumigation off-gas for a more environmentally friendly and safer utilization of SO_2F_2.

In this work, first, the state of the art of SO_2F_2 separation from air is reviewed, and a critical evaluation of the most promising separation processes is provided. Further, this study presents the first detailed experimental characterization of commercial adsorbents for the recovery of SO_2F_2 from dry and humid air. Starting with a screening of four commercial adsorbents for the potential of recovery of SO_2F_2 from air, the hydrophobic zeolite UOP HiSiv 3000 (HiSiv) was chosen for a detailed characterization. Adsorption isotherms on the selected adsorbents in a temperature range of 10–90 °C were measured, which can be used to design temperature swing adsorption (TSA) at practically relevant conditions for the treatment of typical fumigation exhaust air mixtures. Additional dynamic adsorption experiments at process-like superficial velocities were conducted at bench scale to characterize the mass transfer rates of SO_2F_2 adsorption on commercial adsorbents. Finally, results from this work and literature data are combined to form a detailed characterization of HiSiv for adsorptive recovery of SO_2F_2 from air to facilitate the design of gas adsorption processes. Based on this data, a shortcut calculation for an exemplary adsorber design is presented.

2. Separation of SO_2F_2 from air – Preselection of unit operations

In this section, the state of the art of SO_2F_2 recovery methods is summarized and critically evaluated to identify the most promising ones for practical implementation in fumigation gas recovery. Complementary, a brief overview of relevant patents is given in the supporting information (SI) (Tab. S1).

2.1. Thermal decomposition of SO_2F_2

SO_2F_2 is reported to be chemically stable up to temperatures of at least 400 °C [16], (according to other sources, 500 °C [17]) in a completely dry atmosphere, and up to 150 °C in humid conditions [18]. Accordingly, research on controlled decomposition of SO_2F_2 from fumigation gas exhaust by thermal decomposition at 800–1000 °C [19] and plasma-treatment/dielectric barrier discharge (DBD) [20–22] has been published. In these approaches, SO_2F_2 is partly decomposed in the gas phase, which leads to mixtures with harmful decomposition products like HF, F_2 (heat treatment), and SOF_2, SO_2 (DBD). Those in turn should be removed by additional separation steps prior to emission of the off-gas, merely shifting the separation task to other compounds.

2.2. Chemical absorption of SO_2F_2

SO_2F_2 is hydrolysed in aqueous alkaline solution [23,24], which motivated research on chemical absorption [25,26]. Even some partially published studies on chemical absorption in pilot scale exist, e.g. [27, 28], this topic was, however, not followed up upon until now. While up to 95 % of SO_2F_2 could be decomposed in pilot-scale experiments [28], the scrubbing solution, e.g., concentrated aqueous sodium hydroxide (NaOH) or hydrogen peroxide (H_2O_2), has to be periodically replenished. While some research on electrochemical regeneration scrubbing solution exists, this approach is still far from economic feasibility [29]. Finally, chemical absorption of SO_2F_2 produces wastewater with high salt content containing sulphur and fluoride, which must be properly disposed of.

2.3. Physical absorption of SO_2F_2

Physical absorption was studied as a non-destructive separation of SO_2F_2 from air [30–33]. All published studies remain laboratory scale and revolve around the use of organic solvents, which themselves need to be separated from the off-gas streams. In a preliminary rating of the tested solvents for SO_2F_2 based on literature data only, gamma-butyrolactone can currently be proposed as a candidate for the physical absorption of SO_2F_2 from fumigation exhaust air (Table 2). However, due to the inherent contamination of the cleaned air and the enriched SO_2F_2 with solvent, the use of organic scrubbing liquids is generally not recommended for this process. The additional solvent recovery steps would complicate the process further, diminishing economic feasibility.

The following section describes the technical parameters that are used to evaluate possible solvents for SO_2F_2. To design an absorption process, the gas solubility in the solvent must be known as a function of pressure and temperature. The solubility of gases in liquids can be described above and below the critical temperature of the gas using Henry's law [35]. At low pressures $P < 10$ bar and low gas solubilities $x_i < 0.03$ under the assumption of ideal gas behaviour, the gas-liquid equilibrium is approximated by Eq. 1, with the gas mole fraction y_i and the partial pressure p_i of component i.

$$x_i \quad H_{i,\ j}(T) = y_i \quad P = p_i \tag{1}$$

For the practical evaluation of different solvents, it is useful to calculate and compare the technical solubility coefficient $\lambda_{i,j}$, defined as the volume $V_{STP,i}$ of the dissolved gas i at "Standard temperature and pressure" (STP) (273.15 K, 1.013 bar), in relation to the mass m_j of the solvent j and the partial pressure p_i of the gas [35] (Eq. 2).

$$\lambda_{i,\ j} = \frac{V_{STP,i}}{m_j \quad p_i} \tag{2}$$

The technical solubility coefficient can be calculated from the Henry coefficient via Eq. 3 [35]. In principle, this value should be as high as possible, as this means that less volume of solvent is required to absorb the gas, which saves on investment and operating costs (apparatus size, pump capacity, etc.).

$$\lambda_{i,\ j} = \frac{22.41\ \frac{L}{mol}}{M_j \quad H_{i,\ j}(T)} \tag{3}$$

For solvent regeneration and recovery of the absorbed gas, the generally decreasing gas solubility at higher temperatures can be utilized. The temperature dependence of the solubility $\Lambda_{i,j}$ can be represented as a ratio of the technical solubility at different temperatures, coinciding with the ratio of Henry constants at these temperatures (Eq. 4). To ensure efficient desorption, this value should be as far from one as possible.

$$\Lambda_{i,\ j} = \frac{\lambda_{i,\ j}(T_1)}{\lambda_{i,\ j}(T_2)} = \frac{H_{i,\ j}(T_1)}{H_{i,\ j}(T_2)} \tag{4}$$

A suitable solvent for absorption of SO_2F_2 from air should selectively absorb SO_2F_2 in the presence of major air components like N_2 and O_2. The selectivity $S_{i,k}$, sometimes called "separation factor" in equilibrium separation, is classically defined as the ratio of partitioning coefficients x_i/y_i of two components i and k (Eq. 5) [36].

$$S_{i,k} = \frac{x_i \quad y_k}{y_i \quad x_k} \tag{5}$$

To evaluate the suitability of a solvent for physical absorption in a particular use case, Barnicki and Fair suggest using the "solvent selectivity" $\check{S}_{i,k}$ defined as the ratio of the solubilities x_i of the gas components i and k [37]. To achieve efficient separation of the gas mixture, the solvent selectivity towards the target component should be as high as possible. Henry's law only describes binary systems (a pure gas and a

Table 2
Comparison of solvents with known solubility parameters for SO_2F_2.

Solvent	CAS	Technical (literature data, see SI, **Tab. S2**)				Safety [37]		Toxicity [37]		Environment [37]		
		λ(20 °C)	λ(20 °C)/λ(40 °C)	$\check{S}_{SO2F2,N2}$ c)	$\check{S}_{SO2F2,O2}$ c)	T^{LV}	T_{Flash}	LD_{50} oral (rat)	LD_{50} dermal (rabbit)	$c^{TA\text{-}Luft}$	$\dot{m}^{TA\text{-}Luft}$	WGK
		[L_{STP} kg^{-1} bar^{-1}]	[-]	[-]	[-]	[°C]	[°C]	[mg kg^{-1}]	[mg kg^{-1}]	[mg m^{-3}]	[kg h^{-1}]	[-]
dibutyl succinate	141-03-7	3.5	1.16	1.7	3.2	275	135	8000	-	50	5	1
diethyl succinate	123-25-1	3.9	1.19	2.2	4.1	217	94	8530	-	50	5	2
gamma-butyrolactone	96-48-0	2.5	1.19	4.1	6.6	204	94	1540	-	50	5	1
gamma-valerolactone	108-29-2	3.1	1.20	3.7	5.4	207	96	8800	5000	50	5	2
butyl levulinate	2052-15-5	3.7	1.18	2.1	3.9	238	92	-	-	-	-	2
ethyl levulinate	539-88-8	3.8	1.18	2.3	4.7	206	94	5000	5000	50	5	2
methyl laurate	111-82-0	3.6	1.16	1.5	2.6	267	125	-	-	50	5	3
Bis(2-ethylhexyl) azelate	103-24-2	2.5	1.50	1.6	2.7	237	211	-	-	-	-	0
(2-butoxyethyl) acetate	112-07-2	4.3	1.17	-	-	192	74	2400	1500	50	5	1
3-methoxybutyl acetate	4435-53-4	5.0	1.19	-	-	135	60	4210	-	50	5	1
2-methoxyethyl acetate a)	110-49-6	4.8	1.17	-	-	145	47	2900	5300	-	-	1
1-methoxy-2-propylacetate	108-65-6	5.3	1.21	-	-	146	45	8530	5000	50	5	1
diethylene glycol monoethyl ether acetate	112-15-2	3.3	1.18	-	-	219	107	11000	15300	50	5	1
propylene carbonate	108-32-7	2.4	1.20	-	-	242	116	34600	23800	50	5	1
N-methyl-2-pyrrolidone a)	872-50-4	2.4	1.19	-	-	202	86	3910	8000	?	?	1
tributyl phosphate b)	126-73-8	3.2	1.20	-	-	289	154	3000	3100	20	0.1	2
water	7732-18-5	0.2	-	-	-	100	-	-	-	-	-	-

a) Included in the REACH candidate list of "Substances of Very High Concern" [34], b) cancerogenic, relative qualitative ranking of solvent parameters via continuous colour scale from green (positive) over yellow to red (negative), grey: unknown, c) Solvent selectivities with representative ternary feed mixture with molar fractions y_i of 0.780/0.195/0.025 ($N_2/O_2/SO_2F_2$) at 30 °C.

pure solvent); however, from the Henry coefficients of different gas components in the same solvent, the selectivity can be estimated via Eq. 6 [36]. For enrichment or sharp separation of a gas component, the selectivity estimated in this way should be greater than 3–4 [37].

$$\check{S}_{i,k} = \frac{x_i}{x_k} = \frac{H_{i,\ j}(T)p_j}{H_{k,\ j}(T)\ p_i} \tag{6}$$

The above-mentioned technical parameters were calculated from literature data of Henry coefficients for various solvents tested for the physical absorption of SO_2F_2 in literature (Tab. S2) and collected in Table 2. The solvent selectivities were calculated for a representative ternary feed mixture with molar fractions y_i of 0.780/0.195/0.025 ($N_2/O_2/SO_2F_2$) at 30 °C. Additionally, relevant process safety, environmental, and toxicity parameters were collected for the solvents: the boiling point under standard conditions T^{LV}, the solvent's flash point T_{Flash}, oral and dermal lethal doses for 50 % of test subjects LD_{50}, the emission limits in concentration and the "Wasser Gefährdungsklasse (WGK)" (eng. "water hazard class") with a scale from 0 to 3 (water hazard classes: 0 not harmful, 1 slightly harmful, 2 harmful, 3 strongly harmful) (Table 2). The numerical values in each column are marked with different colours (green: positive, red: negative, grey: unknown) for ease of comparison.

Water, with a technical solubility for SO_2F_2 of 0.2 L_{STP} kg^{-1} bar^{-1}, is one order of magnitude lower than the organic solvents (2.4–5.3 L_{STP} kg^{-1} bar^{-1}), rendering it infeasible as a physical solvent, despite its environmental and safety advantages. 2-methoxyethyl acetate and N-methyl-2-pyrrolidone are on the candidate list "registration, evaluation, authorization and restriction of chemicals" (REACH) of substances of very high concern, and tributyl phosphate is considered carcinogenic. Thus, these three solvents are deemed unsuitable. Of the remaining solvents, diethyl succinate, gamma-butyrolactone, gamma-valerolactone, butyl levulinate, ethyl levulinate and methyl laurate are excluded from further consideration due to a WGK of 2 or "harmful". Furthermore, (2-butoxyethyl)acetate, 1-methoxy-2-propyl acetate, and 3-methoxybutyl acetate are excluded due to their flash points below 90 °C, as reaching such temperatures could be considered for desorption, while reaching the flash point in a process must be avoided.

Of the remaining solvents, only gamma-butyrolactone exhibits a selectivity for SO_2F_2 of approximately 4 towards the main component N_2 in the exhaust air. For diethylene glycol monoethyl ether acetate and propylene carbonate, the selectivity could not be calculated due to a lack of solubility data. Therefore, we conclude that only gamma-butyrolactone can currently be proposed as a feasible candidate for the physical absorption of SO_2F_2 from fumigation exhaust air.

2.4. Partial condensation of SO_2F_2

High differences in vapor pressure of SO_2F_2 and the main components of air – nitrogen (N_2) and oxygen (O_2) – suggest partial condensation for their separation (Fig. 1, A). This has been addressed in some patents [38,39] but remains unattractive as a primary separation step due to the required removal of humidity, which precipitates before the condensation of SO_2F_2, and the low temperatures required to reach sufficiently low remaining concentrations in the treated air. In the patents, liquid nitrogen is suggested as a cooling medium, which complicates the handling and is likely uneconomical for this purpose. At

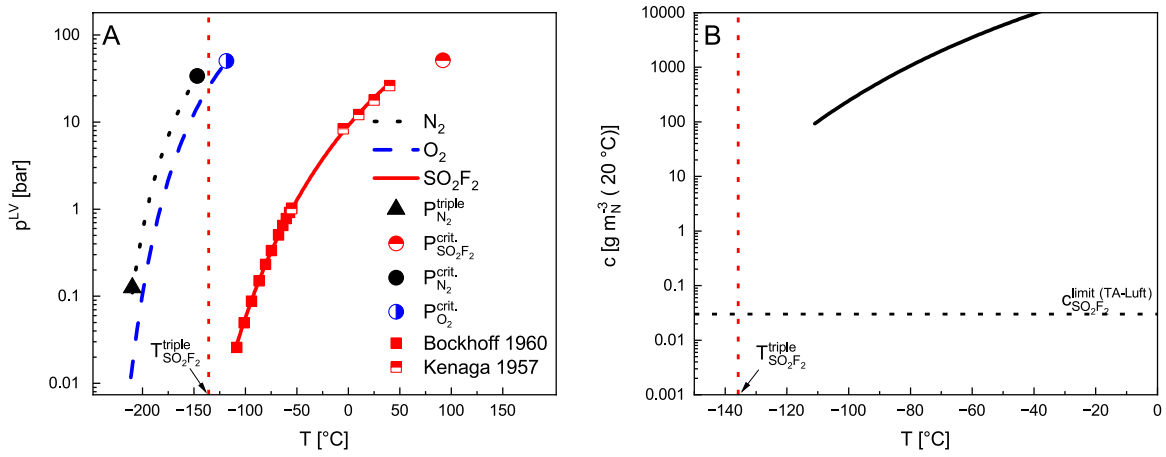

Fig. 1. A) Vapor pressures of SO_2F_2, N_2 [40], and O_2 [41], dotted line: triple point temperature of SO_2F_2, B) Temperature-dependent saturation concentration of SO_2F_2, dotted lines: limiting concentration according to TA-Luft [10] and triple point temperature of SO_2F_2.

ambient pressure, the temperatures required to start the condensation of SO_2F_2 from fumigation atmosphere with 100 g m^{-3} SO_2F_2 begin at −110 °C and will be significantly lower to approach legal limits of 3 mg m^{-3} (TA-Luft, No. 5.2.4 [10]) in the off-gas, making this process unattractive (Fig. 1B).However, partial condensation could be useful in combination with recovering steps like physical adsorption for the purification of reconcentrated, dry air-SO_2F_2 mixtures.

Vapor pressures p^{LV} can be fitted with the empirical Antoine equation with parameters A, B and C and a reference pressure p_0 (Eq. 7):

$$log_{10}\left(\frac{p^{LV}}{p_0}\right) = A - \frac{B}{T + C} \tag{7}$$

Literature data on vapor pressures of SO_2F_2 (Tab. S3) were used to fit a simplified Antoine equation with fixed parameter C to 0. Nitrogen (N_2), oxygen (O_2), and SO_2F_2 exhibit large differences in the vapor pressure curves (Fig. 1, A), separation by partial condensation. By lowering the temperature and possibly increasing the pressure, SO_2F_2 would selectively condense. The most important question is initially up to which temperatures the exhaust air must be lowered to initiate partial condensation of SO_2F_2. To precipitate a specific component from a gas mixture, it must be supersaturated with this component. Under the assumption of Raoult's law, this means that the partial pressure P_i of component i must exceed the vapor pressure p^{LV} of its pure substance at the same temperature (Eq. 8).

$$p_i = P \cdot y_i \geq p^{LV} \tag{8}$$

Assuming ideal gas behavior, the saturation concentration $c(T)$ of a vapor can be estimated from the pure substance vapor pressure $p^{LV}(T)$ when changing the temperature from a reference temperature T_{ref} to T (Eq. 9).

$$c(T) = \frac{p^{LV}(T)}{R} \frac{M_i}{T_{ref}} \tag{9}$$

Eq. 8 can be used to visualize the required condensation temperatures at 1.013 bar to reach certain SO_2F_2 concentrations in air at reference conditions ($T_{ref.}$ = 20 °C and P_{ref} = 1.013 bar) (Fig. 1, B). Condensation of SO_2F_2 at typical fumigation concentrations around 100 g m^{-3} starts below −100 °C, while available data on the vapor pressure of SO_2F_2 ends at a minimum temperature of −109 °C. As extrapolation of the empirical Antoine equation is not recommended, the temperature required for saturation down to a limit concentration of 3 mg m^{-3} SO_2F_2 prescribed by TA-Luft, No 5.2.4 [10] cannot be read directly from the diagram. However, due to the proximity to the triple point temperature of SO_2F_2 at −135.8 °C [42], it can be assumed that this temperature would have to be undercut for complete purification in accordance with TA Luft (max. 3 mg m^{-3})[10]. Since below the triple point temperature, a solid-gas equilibrium is established, the vapor would have to resublime. Thus, a continuous operation would require multiple heat exchangers to periodically purge solid SO_2F_2. As moisture also solidifies temperatures well below 0 °C, partial condensation should be preceded by dehydration of the exhaust air.

2.5. Adsorption of SO_2F_2 from air

Direct adsorption from the gas phase is a promising basis for an emission reduction or even recycling of SO_2F_2 in fumigation and has been analogously implemented for fumigation gas treatment with other gases like methyl bromide [43–46]. According to patents, selective adsorption of SO_2F_2 from mixtures with nitrogen is possible with hydrophobic zeolites with a SiO_2-Al_2O_3 ratio above 10 [47]. However, this is the only published adsorption data on separating SO_2F_2 from air for non-analytical purposes. Further, some coconut shell-derived activated carbons [48], carbon molecular sieves [49] used for analytical methods, and polymer resins [50] are reported to selectively adsorb SO_2F_2. Finally, recent theoretical work found that platinum-doping could enhance the affinity of covalent triazine frameworks for SO_2F_2 [51]. Thus, currently, the development of adsorption processes for SO_2F_2 is hindered by the lack of identification of suitable adsorbents for the selective recovery of SO_2F_2 from air on a technical scale and their experimental characterization.

In this work adsorption of SO_2F_2 on several commercially available and technically feasible adsorbents is experimentally studied, and its potential for the complete recovery process is discussed.

3. Experimental

To close the data gap, preventing a conceptual design of SO_2F_2 adsorption, a number of commercially available adsorbents for off-gas treatment were investigated for their potential to separate SO_2F_2 from dry and humid air. Dynamic adsorption experiments of SO_2F_2 in synthetic air (synth. air) and Helium (He) as carrier gas were used for a screening of all adsorbents. The most promising candidate was picked for a detailed characterization, including the measurement of SO_2F_2 isotherms and mass transfer rates by dynamic measurements in carrier gas.

3.1. Materials

The following four commercially available adsorbents were chosen for screening, based on analysis of available literature for adsorbents selective for SO_2F_2:

1. Hydrophobic zeolite: UOP HiSiv 3000 (Kurt Obermeier Chemie GmbH)
2. Activated carbon: Air CC 816 (Aqua Air Adsorbens GmbH & Co.KG)
3. Activated coke: DGF 3 Super (CarboTech AC GmbH).
4. Activated coke (impregnated): D47/3 KC10 (CarboTech AC GmbH).

UOP HiSiv 3000 (HiSiv) is a zeolite with a high silica to alumina ratio (> 1000), typically used for the removal of volatile organic compounds (VOC) from dry and humid air [52]. Air CC 816 (Air CC) and DGF 3 Super are coconut charcoal and hard coal-based adsorbents, respectively activated by steam and both are marketed for VOC removal [53,54]. D47/3 KC10 (KC10) is a hard coal-based adsorbent impregnated with 10 wt% potassium carbonate (K_2CO_3) and is used for the adsorption of acidic gases [55,56]. All adsorbents feature similar particle sizes: HiSiv in pellets with dimensions of 4 × 1.59 mm, Air CC granular particles with diameters of approx. 2.36–1.18 mm (USS-mesh 8 ×16) and DGF 3 Super and KC10 pelleted with dimensions of 4.7 × 3 mm. Additionally, a chitosan-based carbon aerogel in the form of 1 mm spheres was included in the adsorber screening and compared to the commercial adsorbents.

Pure gases N_2 5.0, CO_2 4.5, synth. air and He 5.0 were obtained from Westfalen AG. Calibration gas mixtures with 1 vol% (±0.01 vol%) SO_2F_2, 3 vol% (±0.03 vol%) SO_2F_2 in synth. air and 3 vol% (±0.03 vol %) SO_2F_2 in He were supplied by Linde Gas GmbH. For experiments with humid air, deionized laboratory water from a central building supply was used.

3.2. Pore size distributions

To characterize the textural properties in the micro- and meso-pore ranges of the investigated adsorbents, gas physisorption experiments with N_2 5.0 at 77 K and CO_2 4.5 at 273 K were conducted. Constant temperatures during measurements were ensured by submerging the samples in liquid nitrogen (N_2 physisorption, 77 K) or water crushed-ice mixtures (CO_2 physisorption, 273 K). An overall sample mass of approx. 20 mg was used in each run, and all samples were degassed at 150 °C (in case of carbons) or 300 °C (in case of zeolites) under vacuum (< 7 mbar) for at least 12 h prior to each analysis. The respective isotherms were determined with a gas sorption analyser (Nova 4200e, Quantachrome) by a manometric method from 5 mbar to ambient pressure.

Pore size distributions were derived by the Barrett-Joyner-Halenda (BJH) method for the meso (2–50 nm) and lower macro (> 50 nm) pore range from the N_2 isotherms and via the Horváth-Kawazoe (HK) and Saito-Foley (SF) method for the micro pore range from CO_2 isotherms. While the HK method, which assumes slit-shaped pores, was applied to the activated carbon samples, the SF method, which assumes cylindrical pores, was applied to HiSiv, which is expected to better fit its micro pore geometry as a ZSM-5 zeolite.

3.3. Dynamic adsorption of SO_2F_2

All dynamic adsorption experiments were conducted in a bench-scale commercial adsorber set-up "mixSorb L" (3 P Instruments GmbH & Co. KG) with added periphery for the detection of SO_2F_2 and relative humidity (RH) at the exhaust (Fig. 2). The whole set-up was placed in a fume hood and constantly monitored for SO_2F_2 by a leakage sensor M.A. C 2640 CLIRcheck (ppm Messtechnik GmbH) (Fig. S1).

The adsorber column consisted of a stainless-steel tube with an inner diameter of 30 mm, an internal length of 200 mm, and a 5 mm thick sintered metal frit as a diffusor on the bottom. It features four Pt100 temperature probes radially centred and positioned 40 mm apart along the column axis. The column was manually filled with adsorbent under gentle shaking to ensure high packing densities. Approximately 15 mm space was left free on the top of the packing to accommodate a quartz wool pad as a dust filter held by a stainless-steel gauze. After sealing the adsorber and connecting it to the mixSorb L, the system was purged and pressurized to 7 bar with He to measure the pressure drop over 2 min to ensure a leakage rate of less than 0.002 mbar L s^{-1}. In case of failure, the connections were retightened and the leak test repeated until passing the test.

Before experiments with a fresh adsorbent sample and in between adsorption experiments, the adsorbent was pretreated in-situ to remove adsorbed humidity. For this, the sample was heated with an external electrical heating mantle, while constantly purging with 500 mL min^{-1} carrier gas. He was used as a purge gas before experiments that used He as a carrier gas. N_2 was used as purge gas for experiments with synth air as carrier gas, accordingly. Zeolite samples were heated at a rate of 2 °C min^{-1} up to 400 °C with a holding time of 4 h. Carbon samples were heated to 150 °C with a rate of 5 °C min^{-1} and held at 150 °C for 2 h. Higher maximum temperatures in the preparation of zeolite samples were chosen to ensure complete removal of bound water molecules (compare [57]). Finally, the adsorbent was allowed to cool to room temperature while purging with gas. Blank corrections were experimentally measured with glass beads as inert filler and are described in the SI (Fig. S3).

For the detection of SO_2F_2 at the adsorber outlet, a constant flow of 1000 mL min^{-1} was branched off from the total exhaust stream via a T-connector by manually regulating with a needle valve and a flow meter

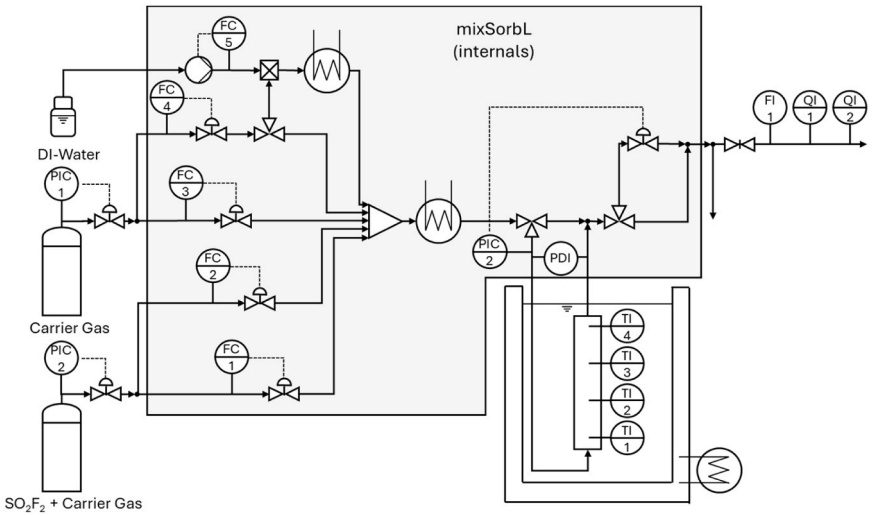

Fig. 2. Sketch of experimental set-up used for dynamic sorption experiments.

GFM mass flow meter (Analyt GmbH & Co. KG). This gas stream was passed over a set of dual-wavelength, non-dispersive infra-red (NDIR) sensors, first over a SO_2F_2 Flowmodule 4 % F3–412406–05000 (smartGAS Mikrosensorik GmbH, "QI 1" in Fig. 2). The sensor has a measurement range of 0 – 4 vol% for SO_2F_2 with a lower limit of detection of $\leq$ 0.004 vol% (3σ) and a straight line deviation of $\leq$ 0.04 vol%. Cross-sensitivities for other infrared-absorbing gases like water are mitigated internally by the simultaneous measurement of a reference wavelength not strongly absorbed by SO_2F_2 (dual wavelength). Additionally, the gas was passed over a SO_2F_2 Flowmodule 100 ppm F3–412104–05000 (smartGAS Mikrosensorik GmbH, "QI 2" in Fig. 2. All external gas flow connections were realised via 1/4 " and 1/8 " stainless-steel tubing (Hy-Lok D Vertriebs GmbH). As the used SO_2F_2 mixtures were calibrating gas quality and the used mix Sorb L offered precise gas dosing via precise mass flow meters (uncertainty < 0.02 % of max. range), the SO_2F_2 sensor could checked and if required calibrated for each experiment via bypass measurements of carrier gas or carrier gas mixtures (He, synth. air, synth. air + water) and the SO_2F_2 calibrating gas.

The temperature of the adsorber column and its feed pipe was controlled by submerging the adsorber cell in a water-filled, double-walled beaker connected to a refrigerating/heating bath MX7LR-20-V12V (VWR International, LLC) using water as a circulating medium. The adsorber pressure during measurements was controlled via an integrated backpressure regulator. For the precise dosing of gases, four in-built Coriolis mass flow controllers (1, 5, 10, and 20 L min^{-1}) were used in connection with double-stage pressure regulators FM53 (Spectron Gas Control Systems GmbH) set at 15 bar. Volumetric flow rates are given for a reference state "Standard temperature and pressure" (STP) (273.15 K, 1.013 bar). For experiments including humidity, water vapor was added to the carrier gas in an in-built vapor dosing system, mixing a precisely controlled liquid water flow via a fifth Coriolis mass flow meter in a heated chamber.

Before each experiment, the adsorber was conditioned by driving carrier gas with a 5 L min^{-1} flow through the adsorber, followed by 10 min of conditioning the feed gas by bypassing the adsorber cell. The feed volume fraction of SO_2F_2 φ_0, was taken at the end of this conditioning. The experiments were started by switching the feed gas mixtures from bypass to the adsorbent cell. During the measurements, the adsorbent bed temperatures T_1-T_4, the volume fraction of SO_2F_2 at the outlet $\varphi(t)$ were observed. Measurements were stopped upon reaching steady state conditions with respect to adsorbent bed temperatures and SO_2F_2 concentration at the outlet.

Under the assumption of ideal gas, the partial pressure of SO_2F_2 in the feed gas p_{SO2F2} was calculated by multiplication of the measured total pressure P in the adsorber cell and the measured concentration from the feed gas mixture φ_0 measured in bypass before each experiment (Eq. 10).

$$p_{SO_2F_2} = P \cdot \varphi_0 \tag{10}$$

The total adsorbed mass of SO_2F_2 m_{SO2F2} was calculated from the mass balance of the adsorber from start time t_0 to the end of the experiment t_{end}, with the volumetric feed flow F_{STP} at standard pressure P_{STP} and temperature T_{STP}, the molecular mass of SO_2F_2 M_{SO2F2}, the ideal gas constant R and numerical integration of the SO_2F_2 outlet concentration $\varphi(t)$ over the adsorption time t (Eq. 11).

$$m_{ads} = \frac{F_{STP}}{R} \frac{P_{STP}}{T_{STP}} M_{SO_2F_2} \left(\varphi_0 \quad (t_{end} - t_0) - \int_{t_0}^{t_{end}} \varphi(t) dt \right) \tag{11}$$

The equilibrium loading q was calculated as the quotient of adsorbed mass of SO_2F_2 m_{ads} and the weighed dry adsorbent mass m_{bed} (Eq. 12).

$$q = \frac{m_{ads}}{m_{bed}} \tag{12}$$

In the dynamic adsorption method, the mass of the adsorbed and desorbed amount of SO_2F_2 is calculated from integrated sensor data. To account for the associated uncertainties, an error propagation analysis was conducted (see SI, section 2.1.4).

3.3.1. Screening experiments

The adsorbents were screened with dynamic sorption experiments and evaluated by four target criteria:

1. Adsorption capacity for SO_2F_2 at 20 °C
2. maximum desorption yield by TSA (max. 95 °C)
3. Adsorption capacity for SO_2F_2 with 80 % RH at 20 °C
4. maximum desorption yield by TSA (max. 95 °C), with 80 % RH at 20 °C

Feeds with concentrations of 0.5 vol%, 1.0 vol%, or 3.0 vol% with a total volume flow of 0.5–5 L min^{-1} were led through the adsorber cell at 20 °C and 1.1–1.6 bar absolute pressure (Tab. S4).

Desorption experiments were started immediately after finishing saturation experiments to check if SO_2F_2 is recoverable from the adsorbents via TSA, indicating whether SO_2F_2 is either physically or chemically adsorbed/converted. For this, the loaded absorber was purged with 0.5 L min^{-1} synth. air while increasing the temperature of the heating bath stepwise up to 95 °C to avoid oversaturation of the 4 vol % SO_2F_2 sensor. Desorption was considered finished when concentrations below 100 ppmv SO_2F_2 were detected at the outlet at 95 °C.

The equilibrium adsorption capacity depends on the partial pressure of SO_2F_2 (p_{SO2F2}), which was varied during screening experiments. Thus, isotherms were fitted to the measured capacities to enable their comparison. For sufficiently low partial pressures, the limiting behaviour of adsorption isotherms on homogeneous surfaces can be described by a linear Henry-type model (Henry regime) [58]. Due to the restricted amount of available screening data, measured at low partial pressures and to avoid overfitting, this single-parameter isotherm was chosen, yielding the Henry constant H_{ads} for comparison of different adsorbents (Eq. 13).

$$q = p_{SO_2F_2} \cdot H_{ads} \tag{13}$$

The desorbed mass of SO_2F_2 m_{des} was calculated from the integral from adsorption start to saturation of the adsorber (Eq. 14).

$$m_{des} = \frac{F_{STP} \cdot P_{STP} \cdot M_{SO_2F_2}}{R \cdot T_{STP}} \cdot \int_{t_0}^{t_{end}} \varphi(t) dt \tag{14}$$

The desorption yield Y was calculated as the quotient of the total desorbed mass of SO_2F_2 and the previously adsorbed mass of SO_2F_2 on the same sample (Eq. 15).

$$Y = \frac{m_{des}}{m_{ads}} \tag{15}$$

In practice, the fumigation atmosphere naturally contains humidity, which may decrease the adsorption capacity for SO_2F_2 and could promote hydrolysis of SO_2F_2 on adsorbents. To investigate these effects, the above-mentioned screening experiments were repeated once per adsorbent with humid air (80 % RH at 20 °C) in the feed.

3.3.2. SO_2F_2 isotherms and adsorption enthalpy

To obtain isotherms for SO_2F_2 on HiSiv, multiple saturation experiments were conducted in direct succession, cumulatively adding SO_2F_2 on the adsorbent. For each new equilibrium point, the SO_2F_2 concentration in the feed was increased in small steps to keep the temperature increase due to adsorption heat small and avoid large changes in flow rate. The software 3 PSim (3 P Instruments GmbH & Co. KG) was used to fit the following isotherm models.

The Langmuir model is a basic and theoretically derived isotherm, which assumes: 1) adsorption on a fixed number of sites, 2) a maximum of one adsorptive per site (monolayer), 3) energetically homogeneous adsorption sites, 4) no interactions between adsorbed molecules. It is suitable to describe mono-layer adsorption and yields the physically meaningful parameters of a finite saturation capacity q_{sat} and an affinity

constant K (Eq. 16) [59].

$$q = q_{sat}\frac{K \quad p_{SO_2F_2}}{1 + K \quad p_{SO_2F_2}} \tag{16}$$

To account for energetically heterogeneous surfaces, as usually encountered in technical adsorbents, the Langmuir isotherm can be expanded to multiple distinct adsorption sites. The simplest multi-site Langmuir model is the dual-site Langmuir isotherm with separate saturation capacities ($q_{sat,A}$, $q_{satx,B}$) and affinity constants (K_A, K_B) for the adsorption sites A and B (Eq. 17) [59].

$$q = q_{\text{sat},\quad A}\frac{K_A \quad p_{SO_2F_2}}{1 + K_A \quad p_{SO_2F_2}} + q_{\text{sat},\quad B}\frac{K_B \quad p_{SO_2F_2}}{1 + K_B \quad p_{SO_2F_2}} \tag{17}$$

Another approach to account for heterogeneous adsorbents is the expansion of the Langmuir model by an empirical heterogeneity parameter θ, as done in the widely used Sips and Toth isotherms. The Sips isotherm can describe heterogeneous adsorbents and finite limits at increasing pressures (Eq. 18). While it can describe finite saturation capacities, it cannot describe the Henry regime (except for the case θ = 1, where it equals the Langmuir isotherm) [59].

$$q = q_{sat}\frac{\left(K \quad p_{SO_2F_2}\right)^{\frac{1}{\theta}}}{1 + \left(K \quad p_{SO_2F_2}\right)^{\frac{1}{\theta}}} \tag{18}$$

The Toth isotherm describes adsorption on heterogeneous surfaces and can describe both, finite saturation capacities and the Henry regime (Eq. 19) [59].

$$q = q_{sat}\frac{K \quad p_{SO_2F_2}}{\left(1 + \left(K \quad p_{SO_2F_2}\right)^{\frac{1}{\theta}}\right)^{\theta}} \tag{19}$$

Physically meaningful parameters are an important benefit of the above-mentioned theoretical and half-empirical models; however, in case they fail to converge, fully empirical models can be used. The Freundlich model is an empirical isotherm, derived from a truncated Taylor-series expansion of the adsorption capacity in powers of the sorptive gas pressure [59]. For a pure component isotherm and truncated after the first term, the two parameters, affinity constant K, and heterogeneity parameter θ, are fitted (Eq. 20). It fails at low pressures, where the slope approaches infinity and cannot describe finite maximum loadings.

$$q = \left(K \quad p_{SO_2F_2}\right)^{\frac{1}{\theta}} \tag{20}$$

To interpolate between isotherms, the temperature dependence of the isotherm parameters can be derived by fitting multiple isotherms at sufficiently near temperatures using a Clausius-Clapeyron-like approach (Eq. 21) [60]. This method requires a triplet of high-quality isotherms at sufficiently similar temperatures to deliver accurate results but also yield the load-dependent adsorption enthalpy Δh^{ads}.

$$\frac{d\left(\ln p_{SO_2F_2}\right)}{d\left(\frac{1}{T}\right)} = -\frac{\Delta h^{ads}}{R} \tag{21}$$

The affinity constant at an interpolation temperature is obtained in relation to a reference affinity constant K_0 at reference temperature T_0 (Eq. 22)

$$K(T) = K_0 \exp\left(-\frac{\Delta h^{ads}}{R}\left(\frac{1}{T} - \frac{1}{T_0}\right)\right) \tag{22}$$

The temperature dependence of the saturation loading is obtained in relation to a reference saturation loading $q_{sat,0}$ at reference temperature T_0, with a constant factor χ (Eq. 23)

$$q_{sat}(T) = q_{sat,\quad 0}\exp\left(\chi\left(1 - \frac{T}{T_0}\right)\right) \tag{23}$$

The temperature dependence heterogeneity parameter is obtained in relation to a reference exponent θ_0 at temperature T_0 by fitting of the factor α (Eq. 24).

$$\frac{1}{\theta}(T) = \frac{1}{\theta_0} + \alpha\left(1 - \frac{T_0}{T}\right) \tag{24}$$

For reference, the adsorption enthalpy was also estimated using the heuristic rule, deriving an estimate of the physical adsorption enthalpy of a gas $\Delta h^{ads,est}$ from its evaporation enthalpy, Δh^{LV} (Eq. 25) [61].

$$1.5 \quad \Delta h^{LV} \leq \Delta h^{ads,est} \leq 2 \quad \Delta h^{LV} \tag{25}$$

3.3.3. Mass-transfer experiments

Additional dynamic adsorption experiments were conducted at increased superficial velocities to characterize the mass transfer rate under realistic conditions. The superficial velocity u was calculated from the feed flow rate F at the controlled temperature T and adsorber pressure P, divided by the cross-sectional area A of the adsorber column (Eq. 26).

$$u = \frac{F(T,P)}{A} \tag{26}$$

3.4. Shortcut method and supporting experiments

A shortcut method is used as a first estimate for a feasible design of an adsorptive SO_2F_2 recovery from fumigation off-gas (see SI, Section 3) [61]. It is based on gathered literature data and the experimental results from this work and should offer an impression of realistic adsorber dimensions, treatment time, and desorption conditions.

An important guideline for the design of fixed-bed adsorbers is the minimum fluidization velocity. It marks the beginning of relative particle movement in a vertical fixed-bed with upward flow. To avoid abrasion, the maximum superficial velocity is often fixed around 50 % of the minimum fluidization velocity [61]. In case of downward flow, higher flow velocities can be safely achieved, which can be utilized in a desorption step. To estimate the minimal fluidization velocities of HiSiv and Air CC, an experimental set-up to measure the pressure drop in dependence on the superficial velocity was used (Fig. S4, A).

3.5. Simulation of breakthrough curves

For the simulation of breakthrough curves, two different programs were used. 3PSim (3 P Instruments GmbH & Co. KG), which allows non-isothermal simulation but is restricted to the dimensions of the mixSorbL laboratory absorber, and Ruptura, which currently only supports isothermal calculations but allows larger adsorber dimensions, useful for scale-up [62]. 3PSim was used to fit a simulation based on the measured isotherms of to an experimental breakthrough curve of SO_2F_2 by variation of the linear driving force (LDF) parameter k_{LDF}. In the LDF approach, the local adsorption rate $\partial q/\partial t$ is proportional to the difference between the equilibrium loading and the locally averaged loading q_x with the mass transfer constant k_{LDF} (Eq. 27) [63].

$$\frac{\partial q}{\partial t} = k_{LDF}(q - q_x) \tag{27}$$

The interstitial gas velocity w is obtained by division of the superficial gas velocity u by the bed porosity ε_{bed} (Eq. 28).

$$w = \frac{u(T,P)}{\varepsilon_{bed}} \tag{28}$$

Dispersion was modelled as plug-flow with an axial dispersion coefficient D_{ax} according to Kast [64] for particle sizes $d_P < 3$ mm (Eq. 29).

$$D_{ax} = w \quad \frac{3 \quad \cdot 10^{-3}}{2} \tag{29}$$

As input, adsorber dimensions, fixed bed properties (Tab. S10), feed conditions (concentration, temperature, pressure, and velocity) and equilibrium parameters were provided (Tab. S11-S13).

4. Results

4.1. Adsorbent screening

The adsorbent screening revealed significant SO_2F_2 capacities below 35 mbar partial pressure of SO_2F_2 on all tested adsorbents (Fig. 3 A). With capacities of up to 80 g kg^{-1}, they lie in the range of literature data for the hydrophobic zeolites Zeocat PZ-2/400 and Wessalith DAZ F20 [47]. Assuming the literature data were measured under ambient pressure (not specified in the reference), the screened adsorbents in this work show steeper slopes (higher Henry constants), indicating higher capacities at low concentrations. (Fig. 3 B). Air CC, DGF 3 Super, and HiSiv feature the highest Henry constants, indicating a high affinity for SO_2F_2. The high uncertainty of 20 % for the Henry constant of DGF 3 Super, compared to the other samples, can be explained by it being based on two measurements at very similar partial pressures of SO_2F_2. Considering the bed densities of HiSiv (700 kg m^{-3}) [52] and Air CC (500 kg m^{-3}) [53], both are equally suitable regarding bed-volume-specific SO_2F_2 capacity.

Under humid conditions, the SO_2F_2 capacity decreased slightly on Air CC, and significantly on DGF 3 Super and HiSiv. On HiSiv, the capacity for SO_2F_2 decreased by 25 %, as expected from general comparison to adsorbent behaviour of adsorbents for VOC recovery from humid air [65] and SO_2F_2-specific literature data on other adsorbents [48]. On the alkaline impregnated coke KC10, humid conditions led to an apparent increase in adsorption capacity. Based on just one measurement, this result suffers from a high uncertainty but could be interpreted as an indication of a promoted chemical conversion of SO_2F_2 by hydrolysis. This is supported by the low desorption yields on the alkaline impregnated KC10, especially low under humid conditions with just 67 % recovery of SO_2F_2 (Fig. 3, C) and matches literature on hydrolysis of SO_2F_2 in alkaline conditions [23,24], which are expected to be induced by the potassium chloride impregnation, typically used to bind acidic gases like HF and SO_2 [56]. At the same time, in dry conditions, SO_2F_2 adsorption on KC10 featured the highest temperature increases (Fig. 6, C), which might be partially explained by the increased feed concentrations of 3 vol% used on this sample but could also, in parts, result from chemical adsorption, which can typically feature ten-fold higher adsorption enthalpies than physisorption [66]. Also, the still rising fixed bed temperatures upon reaching breakthrough conditions on KC10 under humid conditions might be an additional sign of a continuing hydrolysis of SO_2F_2 (Fig. S6, C).

Only HiSiv could repeatedly be fully regenerated by temperature

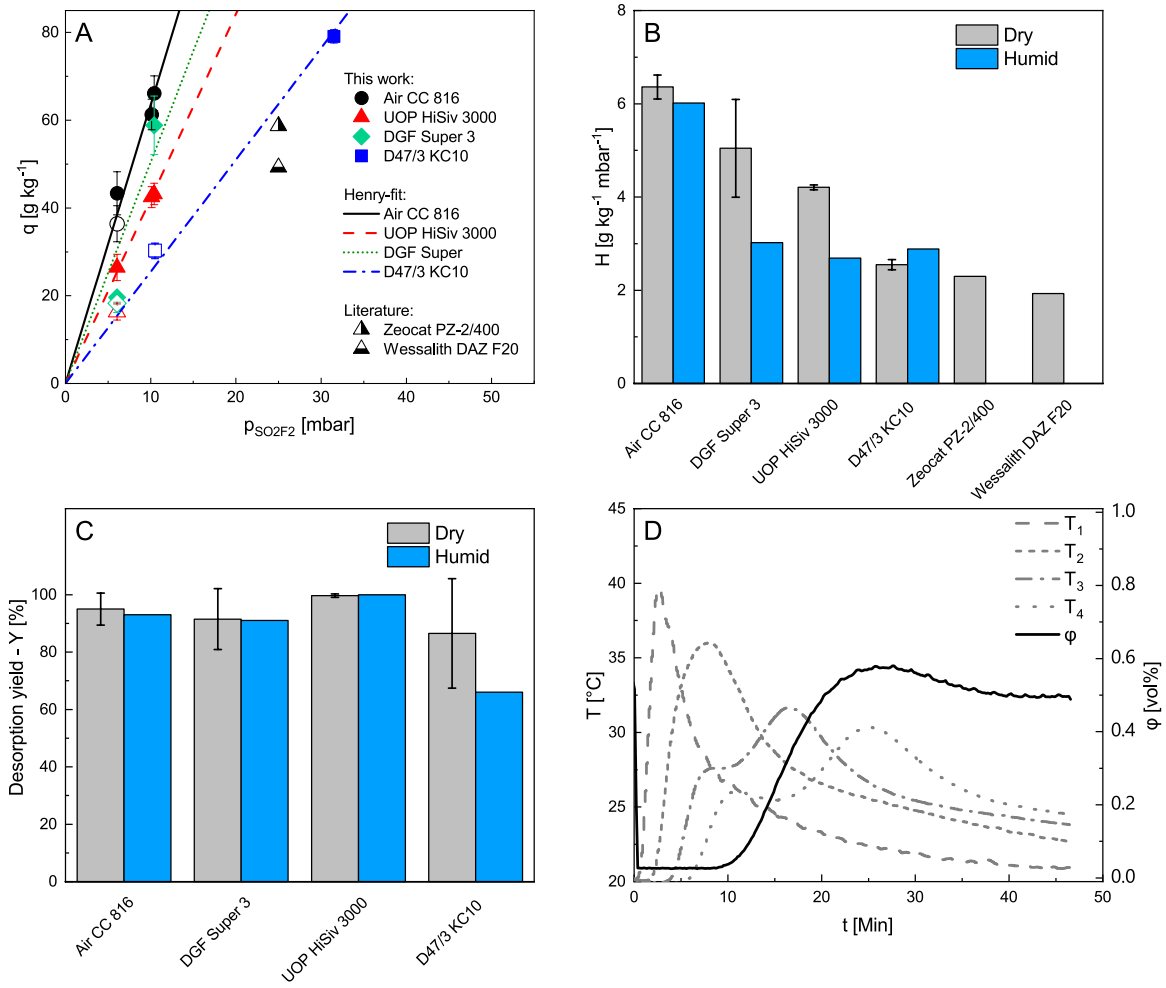

Fig. 3. A) Saturation loadings of SO_2F_2 at 20 °C, empty symbols: capacities in humid conditions, Error bars: uncertainties estimated by error propagation(see SI, section 2.1.5), B) Henry coefficients of SO_2F_2, Error bars: standard error of gradient from linear fit, C) Desorption yield, Error bars from n multiple measurements (n = 2 [DGF 3 Super and D47/3 KC10], n = 3 [UOP HiSiv 3000 and Air CC 816]), D) Breakthrough curve and temperature profile on HiSiv, with: feed conditions: 0.5 vol%, 5 L min^{-1}, 80 % RH.

increase and carrier gas purge, in dry and humid conditions. The incomplete recovery on the carbon adsorbents might be explained by chemical bonding or catalytic decomposition of SO_2F_2 also on the unimpregnated Air CC and DGF 3 Super, as catalytic activity is a commonly occurring characteristic of activated carbons and cokes [65].

On HiSiv, an overshoot of the SO_2F_2 concentration to values above the feed concentrations was observed under humid conditions (Fig. 3, D), which could be caused by different mechanisms, or a mixture thereof. A possible explanation could be the adsorption of H_2O to different sites than SO_2F_2, causing a temporary desorption of already bound SO_2F_2 by temperature increase, while blocking the re-adsorption of SO_2F_2 by steric effects in pore entrances.

Alternatively, the overshoot could be a sign of co-adsorption effects, suggesting that H_2O and SO_2F_2 compete for the same adsorption sites [60]. Under the assumption that SO_2F_2 is transported faster but binds more weakly than H_2O in HiSiv, this overshoot could be the result of H_2O adsorption on sites already occupied by SO_2F_2, leading to the desorption of SO_2F_2, as an enriched SO_2F_2 desorbate pulse. The temperature profiles during this experiment support this hypothesis, as they feature an increasingly pronounced shoulder, splitting off secondary peaks at T_3 and T_4 along the flow direction through the adsorber bed (Fig. 3, D). This indicates the increasingly asynchronous adsorption of multiple adsorptives. The positions of the first temperature peaks roughly coincide with the temperature peaks in pure SO_2F_2 breakthrough under dry and else equal conditions (Fig. S 4, C), indicating their association to SO_2F_2 adsorption. Also, the arrival of the temperature peak at the last sensor T_4 usually roughly coincides with the breakthrough of SO_2F_2 (Fig. S3-S6). In this case, the second temperature peak coincides with the maximum of the SO_2F_2 concentration overshoot. Thus, this second temperature front likely marks the breakthrough of the H_2O front, displacing SO_2F_2 with a net exothermal effect.

To investigate the effect of humidity on adsorption kinetics on the screened adsorbents, SO_2F_2 breakthrough curves from the screening experiments were normalized to feed concentrations and overlayed for dry and humid conditions at equal superficial velocities (Fig. S7). Besides shifts in breakthrough times, the slopes of the concentration profiles were only marginally affected by the added humidity, whereas on HiSiv, the slope steepened, likely due to temperature peaks (Fig. 3, A) and featured the already discussed overshoot of SO_2F_2 concentrations above feed conditions.

Based on the results above, HiSiv was chosen for further characterization as a selective adsorbent for SO_2F_2 from dry and humid air, as it combines high capacities with almost full recoverability of SO_2F_2 in dry and humid conditions. However, also Air CC remains an interesting candidate due to its similar performance. The self-synthesized chitosan-based carbon aerogel showed comparable capacities for SO_2F_2 but low desorption yields of 80 % (Fig. S8).

4.2. Adsorption isotherms SO_2F_2 on HiSiv

Isotherms for SO_2F_2 on HiSiv were measured as step response in He as carrier gas for temperatures of 10–90 °C, likely suitable for a TSA process (Fig. 4, Tab. S5). Even though the isotherms only cover < 1 % of the relative saturation for SO_2F_2, they can be classified as Type I isotherms according to IUPAC nomenclature, which is expected for microporous adsorbents like HiSiv [67]. This also suggests a high affinity between adsorbent and adsorptive, which generally induces a favourable self-sharpening of the breakthrough curve when traveling through an adsorbent bed, increasing its practical capacity during the adsorption step [68].

The experimental uncertainties of the equilibrium loadings estimated by error propagation are dominated by the integrated uncertainty of the SO_2F_2 sensor (see SI, section 2.1.5). Thus, they are very sensitive to the nominal straight-line deviation of the sensor, which was assumed as $\leq$ 0.04 vol% according to the sensor data sheet [69]. While the derived relative uncertainties are well below 5 % for most experiments, single experiments at low temperatures and low partial pressures show relative uncertainties above 70 %. However, the overall isotherm shapes, the expected order of decreasing capacity with increased temperature, and especially the good agreement of the experimental isotherm at 20 °C with saturation capacities calculated from separate breakthrough experiments (Section 3.5) demonstrate experimental reproducibility (Fig. 4, A). Thus, the actual relative errors should be significantly smaller than estimated from error propagation.

To estimate the impact of humidity on the maximum SO_2F_2 capacity, an additional isotherm at 20 °C was measured in synthetic air with 80 % RH. Like in the screening results, a capacity loss for SO_2F_2 of up to 25 % was observed in humid conditions, which likely indicates the potential capacity loss in the treatment of similarly humid fumigation gas mixtures.

All single-component isotherms were used to fit isotherm models, with the isotherms at 10 °C, 20 °C, and 30 °C used to calculate the temperature dependencies and load-dependent adsorption enthalpy Δh^{ads} in the range of 10–30 °C, when possible. The Langmuir adsorption isotherm (LAI) and the Dual-site Langmuir adsorption isotherm (DS-LAI) both converged for simple isotherms (Tab. S6). However, the models failed to deliver sufficient fits to derive temperature dependencies. The half-empirical Toth and Sips models delivered good fits for some single temperatures, but failed for others. Thus, they were not suitable to derive temperature dependencies. As the theoretical and half-empirical

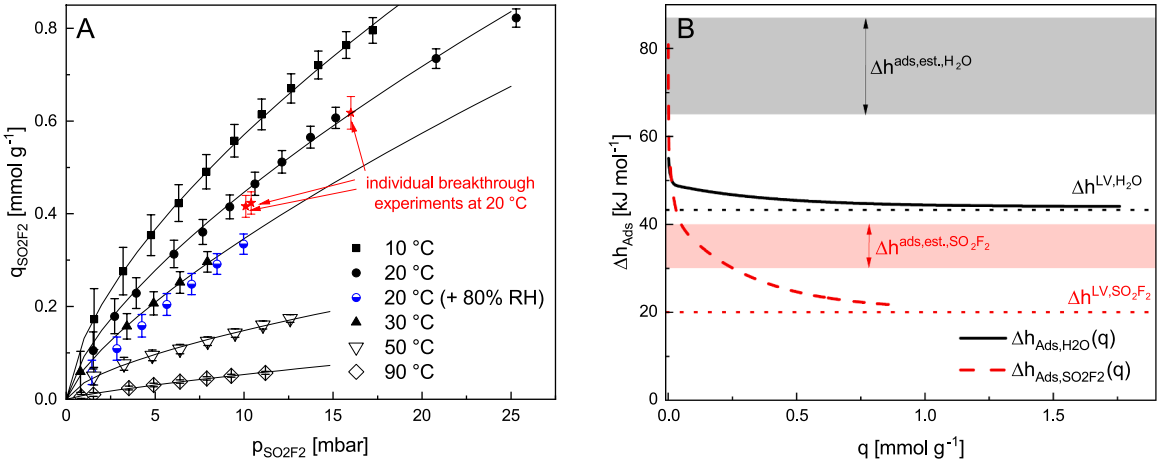

Fig. 4. A) SO_2F_2 isotherms (experimental data and Freundlich fits) on HiSiv, Error bars: uncertainties estimated by error propagation (see SI, section 2.1.5), B) Adsorption enthalpy of SO_2F_2 and H_2O on HiSiv and respective evaporation enthalpies.

models failed to fully describe the experimental isotherms for SO_2F_2 on HiSiv, the empirical Freundlich model was used to describe the isotherms of SO_2F_2 on HiSiv and estimate the load-dependent adsorption enthalpy (Fig. 4, B).

As water is a co-adsorptive in the separation of SO_2F_2 from humid air, literature data on isotherms of water on HiSiv (Tab. S6, Fig. S9) were used to additionally derive the adsorption enthalpy of water on HiSiv. In consistency with theory, the adsorption enthalpies asymptotically approach the respective adsorptive's evaporation enthalpies Δh^{LV} at increased loadings, supporting the accuracy of the derived adsorption enthalpies (Fig. 4, B) [64]. Both for water and SO_2F_2, the estimated adsorption enthalpy according to heuristics (Eq. 19) lies well in the range of the isotherm-derived adsorption enthalpies on HiSiv (Tab. S7), further indicating the results' plausibility. The higher adsorption enthalpy of H_2O in comparison to that of SO_2F_2 on HiSiv further supports the co-adsorption hypothesis, as a higher adsorption enthalpy correlates with a higher affinity to the adsorbent, explaining the observed roll-over effect with H_2O seemingly displacing SO_2F_2 from common adsorption sites (Fig. 3, D) [70].

4.3. Breakthrough curves and mass transfer kinetics

Experiments at various superficial velocities were carried out to estimate the adsorption kinetics under practical conditions. The breakthrough curves of SO_2F_2 on HiSiv and Air CC feature a typical sigmoidal shape with a slight asymmetry (Fig. 5, A), which may be attributed to temporary, local, non-isothermal conditions due to the exothermic adsorption [57]. With increasing flow rates, the slope of the breakthrough curves increases for both adsorbents.

Notably, at equal flow rates, HiSiv features steeper breakthrough curves than Air CC (Fig. 5, A), indicating higher internal mass transfer limitations in Air CC. A possible explanation lies in the nanopore texture, where generally, the presence of connecting macro and mesopores is expected to enhance intraparticle diffusion rates in nanoporous adsorbents [71].

Gas physisorption measurements (Fig. S10, A-D) reveal that Air CC exhibits the lowest meso- (to lower macro-) pore volume of 0.024 mL g^{-1}, while HiSiv shows the highest meso- (to lower macro-) pore volume (0.15 mL g^{-1}) (Fig. 6), in good accord with literature values of 0.169 mL g^{-1} [72]. By comparison of the micropore volumes derived by the HK and SF methods, Air CC exhibits the highest micropore volume (0.132 mL g^{-1}) compared to the remaining adsorbents (0.080–0.085 mL g^{-1}), again for HiSiv in good accord with literature (0.100 mL g^{-1}) [73,74].

Under the assumption that the granular, coconut shell-derived Air CC particles feature homogeneous porosity, the internal mass transport resistance should depend directly on the particle size, directly influencing the diffusion path length to the central pores. The remaining adsorbents are all pelletized, meaning that nanoporous adsorbent particles are mixed with binder materials to create a secondary, often macroporous network, which is likely the source of their increased relative meso- to macro porosity (Fig. S11, C) [75]. Thus, decreasing the particle size of Air CC could decrease intraparticle mass transfer, increasing the technically usable adsorber length by sharpening the mass transfer zone. In practice, however, this has to be balanced out against the pressure drop, which increases with smaller particles [60].

On HiSiv, the measurement at the highest measured flow rate (15 min^{-1} (STP)) featured a superficial velocity of 0.24 m s^{-1} (Tab. S8), coinciding with the determined maximum up-scaled fixed bed gas velocity for upwards flow in a vertical fixed bed for this adsorbent. Thus, this experiment was used to fit the k_{LDF} mass transport coefficient for SO_2F_2 by comparing the breakthrough curve with a simulated experiment, based on the fitted Freundlich isotherms of SO_2F_2 on HiSiv. While the experimental temperature peaks along the fixed bed exceed those of the simulation by 2–5 °C, their peak location in time is well reflected by the simulation (Fig. 5, B). To validate the accordance of the open-source simulation program Ruptura with these results, it was used to simulate the same laboratory experiment with the same parameters. As it shows even better agreement with the experimental data, it is deemed that Ruptura is principally suitable to calculate isothermal adsorption dynamics with SO_2F_2 on HiSiv, also for other scales and geometries, as in the following conceptual design calculations.

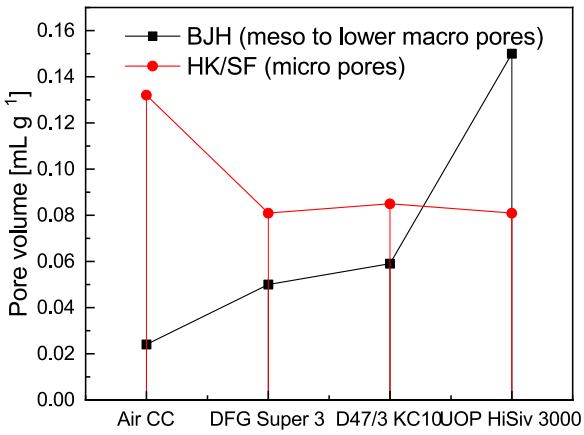

Fig. 6. Total pore volumes in the micro- (HK/SF) and meso- to lower macro pore range (BJH).

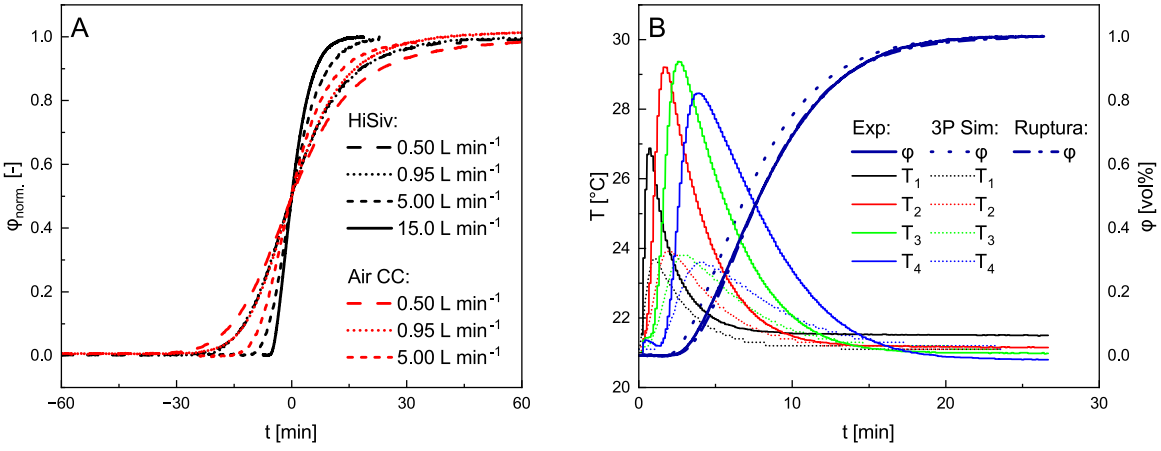

Fig. 5. A) Normalized breakthrough curves of SO_2F_2 on HiSiv and Air CC, B) Fit of breakthrough on HiSiv simulated with 3pSim to experimental curve: k_{LDF} = 0.725 min^{-1} and comparison simulation by Ruptura.

4.4. Conceptual adsorber design

The shortcut calculations yield basic adsorber dimensions and cycle times for a simple TSA (Table 3). While both shortcut designs target breakthrough times of 20 min, these are not exactly matched by the respective simulations, resulting in 15 min (Shortcut 20 °C) and 21 min (Shortcut 10 °C) (Fig. 7). The simulations include an actual quantification of the MTZ, and thus can be deemed more accurate than the shortcut method, where an estimated safety margin of + 50 % adsorber mass was chosen to account for practical capacity reduction of the bed by accommodation of the MTZ and non-isothermal adsorption due to adsorption heat (see SI, section 3.2.1). Based on this result, an increased adsorber length to 0.92 m is recommended to reach 20 min breakthroughs and thus a complete treatment of a container charge in the 20 °C shortcut scenario.

a) Estimated from measurements, b) Estimated from pressure drop calculations, c) Measured, Symbols: T Temperature, φ average feed concentration of SO_2F_2, u_0 superficial gas velocity, m_{ads} adsorbent mass, D adsorbent bed diameter, L adsorbent bed length, t_{ads} adsorption time until breakthrough, T_{des} desorption temperature, t_{des} desorption time, EF enrichment factor of SO_2F_2 in desorbed effluent.

The low predicted enrichment factors EF (Table 3) indicate that a simple hot gas desorption would be inefficient for a reconcentration of SO_2F_2 with HiSiv, as the quantity of purge gas required to heat the fixed bed and desorb SO_2F_2 is equal to or higher than the quantity of treated feed in the adsorption step. To prevent the dilution of SO_2F_2 during desorption, external heating of the fixed bed could be employed.

Alternatively, steam desorption with superheated steam could be employed to displace SO_2F_2 and reconcentrate it in a short pulse of desorbate [65]. Besides high specific enthalpies of steam, which allow desorption with lower dilution of the target component, other than hot air, the steam can be separated from SO_2F_2 by partial condensation for increased enrichments. Desorption by direct application of steam to the loaded adsorbents is a widely used technique for the desorption of activated carbons [27] and is also reported for hydrophobic zeolites [28]. In it, steam is fed either saturated or superheated in a continuous or interrupted manner to the adsorbent bed to heat the adsorbent and displace the adsorbed species.

As an exemplary case, a steam desorption process for SO_2F_2 recovery from the Short Cut case at 20 °C is considered. Condensation and thus desorption, at ambient pressure, is assumed; however, if saturated steam at higher pressures is available, the desorption could principally be conducted at higher temperatures by controlling the pressure in the adsorber during condensation. The process design is based on calculations of the following design (see SI, section 3.2.3) (Fig. 8, A):

1. Generation of saturated steam at T_1 and P_1
2. Isenthalpic throttling to ambient pressure P_2, resulting in superheated steam at $T_2 < T_1$
3. Isobaric cooling of superheated steam and condensation at 1.01 bar, 100 °C

To heat the adsorbent bed 20 °C to 100 °C an energy of 2700 kJ is required (15 % SO_2F_2 desorption, 85 % heating of adsorber). In the extreme case of total condensation ($x_4 = 0$) a minimum of 1.2 kg steam (0.8 kg kg^{-1} steam per SO_2F_2) is required and leaves approximately 3.5 wt% humidity on the adsorbent, depending on the temperature of the generated feed steam. If more superheated steam is fed, more energy

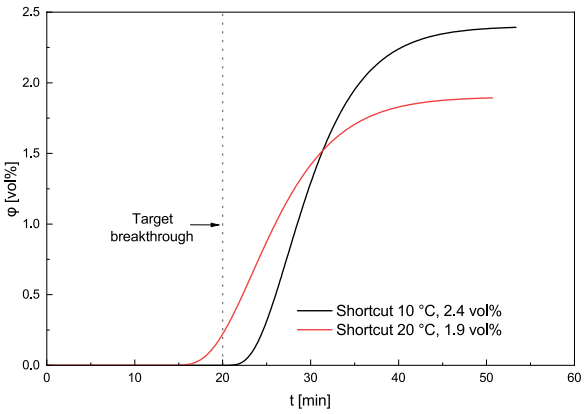

Fig. 7. Simulated breakthrough curves of shortcut designs.

is covered by cooling the superheated steam, instead of condensation, leaving the adsorber in a dryer final state 4 (Fig. 8, B).

As water seems to displace SO_2F_2 on HiSiv as a co-adsorbent, indicated by roll-over effects and higher adsorption enthalpies of water on HiSiv, a facilitated desorption of SO_2F_2 is expected at the cost of an additional drying step, which could be realised, for example, with hot air. For an economic process, incomplete drying would likely have to be employed, decreasing the practical capacity for SO_2F_2 and potentially increasing mass transfer resistances due to pore blockage.

In the proposed processes for adsorptive recovery of SO_2F_2, a long-term exposure of the adsorbents to SO_2F_2 and H_2O is expected, as a complete adsorbent regeneration is typically not economically or even technically feasible. Thermal regeneration of the adsorbent by hot gas or steam could increase the reactivity of SO_2F_2, and the presence of adsorbents could catalyse the degradation of SO_2F_2 to toxic and corrosive products. Thus, the chemical stability of SO_2F_2 in the presence of specific adsorbents, which might act as catalysts, should be experimentally tested at targeted desorption conditions, e.g., in humid air and steam up to temperatures of 150 °C.

Further, it is recommended to experimentally evaluate the adsorbent stability in cyclic adsorption-desorption tests with hot gas and steam desorption. Potential pore blockage or ageing mechanisms during the use of the discussed adsorbents are not easy to predict and should be assessed in long-term cyclic experiments. Zeolites degrade in contact with acids; however, high silica to alumina ratios in hydrophobic zeolites increase acid resistance [76]. UOP HiSiv 3000 has a high silica to alumina ratio, which should increase its resistance against acidic decomposition products of SO_2F_2 [52].

5. Conclusion

After a critical review of the state of the art for SO_2F_2 separation from mixtures with air and a comparison of different separation concepts, including our own experiments, we conclude that direct adsorption of SO_2F_2 from the gas phase is the most promising separation technology for practical implementation in fumigant recovery. Thermal and plasma-induced decomposition of SO_2F_2 is generally incomplete and produces a mixture of toxic and corrosive decomposition products and SO_2F_2, which still need to be separated from the treated air. Decomposition in aqueous alkaline solution (chemisorption) results in safe decomposition

Table 3
Results and parameters of shortcut calculations.

	T	φ	u_0	m_{ads}	D	L	t_{ads}	T_{des}	t_{des}	EF
	[°C]	**[vol%]**	**[m s^{-1}]**	**[kg]**	**[m]**	**[m]**	**[min]**	**[°C]**	**[min]**	**[-]**
Shortcut 10 °C	10	2.4	0.24	33.0	0.29	0.71	20	140	7	0.7
Shortcut 20 °C	20	1.9	0.24	31.8	0.29	0.69 (0.92 m)	20	140	7	1.1

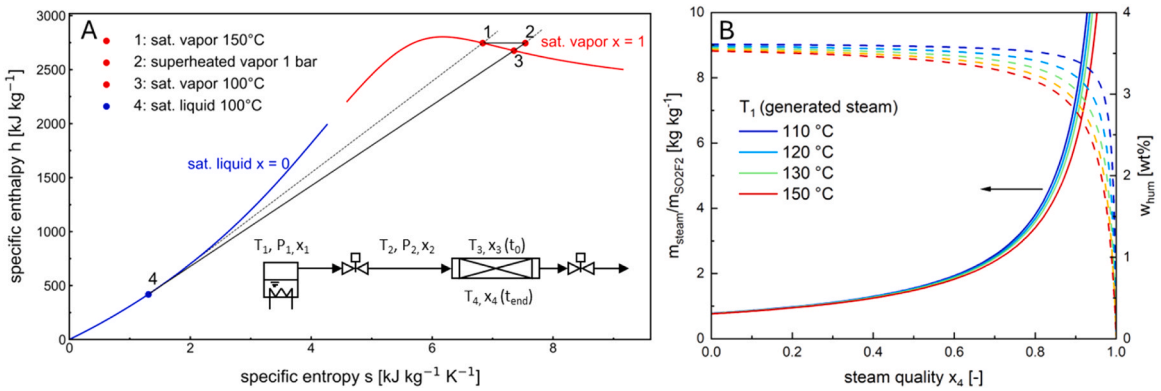

Fig. 8. A) Mollier diagram for water with states of an exemplary steam desorption process, Insert: Process sketch of steam desorption, B) Effect of final steam quality on total steam per SO_2F_2 and remaining humidity in adsorber for different temperatures T_1 of generated feed steam.

products but consumes large amounts of NaOH or hydrogen peroxide, which must be periodically replenished. Also, a complete decomposition has not been achieved in alkaline absorption of SO_2F_2, and the waste management of large amounts of reacted scrubbing waste remains a challenge. Physical absorption and partial condensation both offer the possibility to recover SO_2F_2 for further use. However, physical absorption lacks a suitable solvent to selectively absorb SO_2F_2 from air for reconcentration, and partial condensation of SO_2F_2 requires impractically low temperatures to start condensation of typical fumigation atmospheres, or even to reach legal and safe limits in the treated gas.

Process design of SO_2F_2 adsorption was held back by the lack of publicly available data on suitable adsorbents for SO_2F_2 recovery. In this study, for the first time, a comprehensive experimental evaluation of the adsorption and desorption capabilities of adsorbents for SO_2F_2 under typical fumigation conditions is presented by screening different industrial activated carbons and a hydrophobic zeolite. Among these, the coconut shell-derived activated carbon Air CC and the zeolite HiSiv 3000 were identified as promising materials to recover SO_2F_2 from dry and humid air (80 % RH) at practically relevant temperatures of 20 °C and ambient pressure. Both materials were found to adsorb SO_2F_2 mainly or fully physically, enabling recovery of SO_2F_2 instead of its decomposition to waste compounds.

HiSiv 3000 was further characterized by measuring adsorption isotherms for SO_2F_2 in a temperature range from 10 to 90 °C, fitted by Freundlich isotherms. From these isotherms, the adsorption enthalpy of SO_2F_2 on HiSiv 3000 was calculated and partly validated by comparison with corresponding evaporation enthalpies from literature. Comparisons of experimental breakthrough curves of SO_2F_2 on HiSiv 3000 and Air CC hint at higher mass transfer resistance in Air CC. A fit of an isothermal breakthrough model to an experimental breakthrough curve on HiSiv 3000 yielded a k_{LDF} of 0.75 min^{-1} as the first presented approximation of mass transport during the adsorption of SO_2F_2 from air in a fixed bed.

A conceptual design based on experimental data from this study was realized in the form of shortcut calculations used to estimate adsorber dimensions and process parameters for SO_2F_2 adsorption on HiSiv from venting a fumigated export container. Based on these results, a TSA process with superheated steam as desorption gas seems advantageous over desorption by heated air to reconcentrate SO_2F_2. The observed co-adsorption of SO_2F_2 and H_2O on HiSiv in the form of roll-over effects and high adsorption enthalpies of water could increase the effectiveness of steam desorption. Alternatively, external heating would likely be required to enrich SO_2F_2 via hot-gas desorption.

Air CC is a promising and potentially cheaper alternative to HiSiv 3000, with higher mass-specific capacity for SO_2F_2 in dry and humid states. The apparently higher internal mass transfer resistance of the granular particles could be explained by a lower specific meso-and microporosity, potentially leading to longer diffusion path lengths through micropores. However, incomplete SO_2F_2 recovery on Air CC could indicate partial chemisorption or catalytic decomposition, which should be experimentally investigated to better assess its applicability for SO_2F_2 recovery.

For future studies, it is recommended to experimentally evaluate the stability of SO_2F_2 and the adsorbent microstructure via cyclic adsorption-desorption under elevated temperatures up to 150 °C to assess the long-term stability of SO_2F_2 recovery via hot gas- and steam desorption.

Declaration of Competing Interest

The authors declare that they have no known competing financial interests or personal relationships that could have appeared to influence the work reported in this paper.

Acknowledgments

The authors would like to thank Kurt Obermeier Chemie GmbH for providing the Zeolite UOP HiSiv 3000, Aqua Air Adsorbens GmbH & Co. KG for providing the activated carbon Air CC 816, and CarboTech AC GmbH for supplying the activated cokes DGF 3 Super and D47/3 KC10.

This research was funded by the “Behörde für Umwelt, Klima, Energie und Agrarwirtschaft Hamburg (BUKEA)“ as part of the program “Klimaplan Hamburg“.

Appendix A. Supporting information

Supplementary data associated with this article can be found in the online version at doi:10.1016/j.jece.2025.119270.

Data Availability

Data will be made available on request.

References

[1] D. Stewart, Sulfuryl fluoride—a new fumigant for control of the drywood termite kalotermes minor hagen, J. Econ. Entomol. 50 (1957) 7–11, https://doi.org/10.1093/jee/50.1.7.
[2] Procedure of Ship Fumigation on Import Logs SN/T 2771—2011, (2011). https://cceeccic.org/1125404949.html
[3] Department of Agriculture and Water Resources, Sulfuryl fluoride fumigation methodology, (2018). agriculture.gov.au/publications

[4] Z. Zhang, Use of sulfuryl fluoride as an alternative fumigant to methyl bromide in export log fumigation, N. Z. Plant Prot. 59 (2006) 223–227, https://doi.org/10.30843/nzpp.2006.59.4545.

[5] Report of the technology and economic assessment panel (TEAP): progress report, UNEP, Nairobi, Kenya, 2004

[6] A. Gressent, M. Rigby, A.L. Ganesan, R.G. Prinn, A.J. Manning, J. Mühle, P. K. Salameh, P.B. Krummel, P.J. Fraser, L.P. Steele, B. Mitrevski, R.F. Weiss, C. M. Harth, R.H. Wang, S. O'Doherty, D. Young, S. Park, S. Li, B. Yao, S. Reimann, M. K. Vollmer, M. Maione, J. Arduini, C.R. Lunder, Growing atmospheric emissions of sulfuryl fluoride, J. Geophys. Res. Atmos. 126 (2021), https://doi.org/10.1029/2020JD034327.

[7] Scientific assessment of ozone depletion: 2018, World Meteorological Organization, Geneva, Switzerland, 2019

[8] V.C. Papadimitriou, R.W. Portmann, D.W. Fahey, J. Mühle, R.F. Weiss, J. B. Burkholder, Experimental and theoretical study of the atmospheric chemistry and global warming potential of SO $_2$ f $_2$, J. Phys. Chem. A 112 (2008) 12657–12666, https://doi.org/10.1021/jp806368u.

[9] Regulation (EU) 2024/573 of the European Parliament and of the Council of 7 February 2024 on fluorinated greenhouse gases, amending Directive (EU) 2019/1937 and repealing Regulation (EU) No 517/2014, n.d

[10] Neufassung der Ersten Allgemeinen Verwaltungsvorschrift zum Bundes-Immissionsschutzgesetz (Technische Anleitung zur Reinhaltung der Luft – TA Luft), (2021). https://www.verwaltungsvorschriften-im-internet.de/bsvwvbund_18082021_IGI25025005.htm (accessed June 25, 2025).

[11] Applicator Manual for ProFume® gas fumigant, (2016). https://labelsds.com/images/user_uploads/Profume%20Appl%20Manual%201–1-16.pdf (accessed June 25, 2025)

[12] S. Kümmritz, S. Feltgen, M. Kayka, N. Bräsicke, G. Kroos, B. Hoppe, Klimaneutrale Begasungsverfahren und alternative Behandlungsmethoden für Rundholz im Export - KLIMAtiv - Zwischenergebnisse des JKI, jKi (2024), https://doi.org/10.5073/20240618-095501-0.

[13] J. Tao, Estimating sulfuryl fluoride emissions during structural fumigation of residential houses, Water Air Soil Pollut. 230 (2019) 96, https://doi.org/10.1007/s11270-019-4152-7.

[14] S.A. Cryer, Predicted gas loss of sulfuryl fluoride and methyl bromide during structural fumigation, J. Stored Prod. Res. (2008) 10.

[15] S.A. Cryer, D.E. Barnekow, Estimating outside air concentrations surrounding fumigated grain mills, Biosyst. Eng. 94 (2006) 557–572, https://doi.org/10.1016/j.biosystemseng.2006.03.013.

[16] M.J. O'Neil, P.E. Heckelman, P.H. Dobbelaar, K.J. Roman, C.M. Kenny, L. S. Karaffa, Royal society of chemistry (Great Britain), eds., the merck index: an encyclopedia of chemicals. Drugs, and Biologicals, 15th ed, Royal Society of Chemistry, Cambridge, UK, 2013.

[17] C.R. Worthing, S.B. Walker. British Crop Protection Council, eds., The pesticide manual: a world compendium, 8th ed, British Crop Protection Council, Thornton Heath, 1987.

[18] N. Wiberg, Lehrbuch der anorganischen chemie, De Gruyter, 2008. ⟨https://www.degruyter.com/document/doi/10.1515/9783110206845/html⟩ (accessed February 18, 2021).

[19] G.D. Binker, J. Binker, Verfahren zum Ableiten eines Gas-Luftgemisches aus einem Raum, DE4401338C5, 2006. https://patents.google.com/patent/DE4401338C5/de?q=r%C3%BCckgewinnung&inventor=Gerhard+Dr.+Binker&scholar&oq=inventor:(Gerhard+Dr.+Binker)+r%C3%BCckgewinnung (accessed November 11, 2020).

[20] Y. Nie, Q. Zheng, X. Liang, D. Gu, M. Lu, M. Min, J. Ji, Decomposition treatment of SO $_2$ f $_2$ using packed bed DBD plasma followed by chemical absorption, Environ. Sci. Technol. 47 (2013) 7934–7939, https://doi.org/10.1021/es400786p.

[21] Y. Zhang, M. Wang, C. Zhou, Y. Li, Z. Yang, X. Zhang, Degradation of sulfuryl fluoride by dielectric barrier discharge synergistically with reactive gas, AIP Adv. 14 (2024) 015063, https://doi.org/10.1063/5.0169153.

[22] Y. Li, Z. Yang, K. Wan, L. Yu, H. Tan, X. Zhang, W. Liu, Study on the effect of catalytic degradation of sulfuryl fluoride in air pollutants by DBD filled with SiO2 glass beads, Appl. Surf. Sci. 687 (2025) 162222, https://doi.org/10.1016/j.apsusc.2024.162222.

[23] G.H. Cady, Sudhindra Misra, Hydrolysis of sulfuryl fluoride, Inorg. Chem. 13 (1974) 837–841, https://doi.org/10.1021/ic50134a016.

[24] S.G. Heuser, Volumetric determination of concentrations of sulfuryl fluoride in air, Anal. Chem. 35 (1963) 1476–1479, https://doi.org/10.1021/ac60203a016.

[25] Y. Nie, X. Liang, M. Lu, F. Yu, D. Gu, M. Min, J. Ji, Mass transfer and reaction kinetics of sulfuryl fluoride absorption with aqueous sodium hydroxide solutions, J. Zhejiang Univ. Sci. A 15 (2014) 540–546, https://doi.org/10.1631/jzus.A1400055.

[26] Y. Nie, X. Liang, J. Ji, M. Lu, F. Yu, D. Gu, Q. Xie, M. Min, Harmless treatment of sulfuryl fluoride by chemical absorption, Environ. Eng. Sci. 32 (2015) 789–795, https://doi.org/10.1089/ees.2015.0021.

[27] Die Senatorin für Wirtschaft, Arbeit und Europa Referat Z3 Verwaltungsbehörde des Europäischen Fonds für regionale Entwicklung, europäische Wirtschafts- und Strukturpolitik, redSF - Europäischer Fonds für regionale Entwicklung, Eur. Fonds Für Reg. Entwickl. Brem. (n.d.). https://www.efre-bremen.de/projekte/redsf-37413?asl= (accessed July 10, 2023)

[28] S. Spencer, Sulfuryl Fluoride TASC Project Update, in: Proc. Methyl Bromide Altern. Outreach Res. Conf. Orlando FL, 2022.

[29] C. Weng, C. Napier, C. Katte, S.S. Walse, W.A. Mitch, Electrochemical generation of hydroxide and hydrogen peroxide for hydrolysis of sulfuryl fluoride fumigant, J. Agric. Food Chem. 72 (2024) 15133–15141, https://doi.org/10.1021/acs.jafc.4c00864.

[30] X. Liang, Y. Nie, D. Deng, M. Lu, F. Yu, P. Chen, J. Ji, Solubility and thermodynamic properties of sulfuryl fluoride in water, J. Chem. Thermodyn. 95 (2016) 190–194, https://doi.org/10.1016/j.jct.2015.12.013.

[31] X. Liang, S. Ye, Q. Xie, M. Lu, F. Xia, Y. Nie, Z. Pan, J. Ji, Solubilities of sulfuryl fluoride in propylene carbonate, tributyl phosphate and N-methylpyrrolidone, J. Chem. Thermodyn. 125 (2018) 11–16, https://doi.org/10.1016/j.jct.2018.05.007.

[32] X. Liang, Y. Fei, Q. Xie, M. Lu, Z. Pan, Y. Nie, J. Ji, Solubilities of sulfuryl fluoride in 2-Butoxyethyl acetate, 3-Methoxybutyl acetate, 2-Methoxyethyl acetate, 1-Methoxy-2-propyl acetate, and 2-(2-Ethoxyethoxy)ethyl acetate, J. Chem. Eng. Data 63 (2018) 2271–2279, https://doi.org/10.1021/acs.jced.8b00224.

[33] X. Liang, Y. Fei, Q. Xie, Y. Liu, M. Lu, F. Xia, Y. Nie, J. Ji, Sulfuryl fluoride absorption from fumigation exhaust gas by biobased solvents: thermodynamic and quantum chemical analysis, Ind. Eng. Chem. Res. 58 (2019) 5018–5029, https://doi.org/10.1021/acs.iecr.8b06112.

[34] Substance Infocard - 1-methyl-2-pyrrolidone, (2023). https://echa.europa.eu/sv/substance-information/-/substanceinfo/100.011.662.

[35] D. Lüdecke, Thermodynamik, Springer, 2000.

[36] W.D. Seider, ed., Product and process design principles: synthesis, analysis, and evaluation, 3. ed., international student version, Wiley, Hoboken, NJ, 2010

[37] S.D. Barnicki, J.R. Fair, Separation system synthesis: a knowledge-based approach. 2. gas/vapor mixtures, Ind. Eng. Chem. Res. 31 (1992) 1679–1694, https://doi.org/10.1021/ie00007a014.

[38] G.D. Fröba, Umweltschonendes Begasungsverfahren, DE19708669C5, 2006 (accessed November 11, 2020), ⟨https://patents.google.com/patent/DE19708669C5/de?inventor=Georg+Dr.+Fr%C3%B6ba&scholar⟩.

[39] G.D. Binker, J. Binker, G.D. Fröba, Verfahren und Vorrichtung zur Lüftung begaster Behandlungsräume, DE19747880B4, 2007. https://patents.google.com/patent/DE19747880B4/de?q=r%C3%BCckgewinnung&inventor=Gerhard+Dr.+Binker&scholar&oq=inventor:(Gerhard+Dr.+Binker)+r%C3%BCckgewinnung (accessed November 11, 2020).

[40] M.P. Edejer, G. Thodos, Vapor pressures of liquid nitrogen between the triple and critical points, J. Chem. Eng. Data 12 (1967) 206–209, https://doi.org/10.1021/je60033a014.

[41] G.T. Brower, George Thodos, Vapor pressures of liquid oxygen between the triple point and critical point, J. Chem. Eng. Data 13 (1968) 262–264, https://doi.org/10.1021/je60037a038.

[42] F.J. Bockhoff, R.V. Petrella, E.L. Pace, Thermodynamic properties of sulfuryl fluoride from 12°K to its boiling point. Entropy from molecular and spectroscopic data, J. Chem. Phys. 32 (1960) 799–804, https://doi.org/10.1063/1.1730800.

[43] M. Nagji, Recycling and recovery of methyl bromide fumigant, US5505908A, 1996, (accessed May 7, 2021)⟨https://patents.google.com/patent/US5505908A/en⟩.

[44] W.A. Hall, D.E. Bellamy, S.S. Walse, Activated carbons from End-Products of tree nut and tree fruit production as sorbents for removing methyl bromide in ventilation effluent following postharvest chamber fumigation, J. Agric. Food Chem. 63 (2015) 3094–3103, https://doi.org/10.1021/jf505193e.

[45] J.G. Leesch, G.F. Knapp, B.E. Mackey, Methyl bromide adsorption on activated carbon to control emissions from commodity fumigations, J. Stored Prod. Res. 36 (2000) 65–74, https://doi.org/10.1016/S0022-474X(99)00028-4.

[46] J.D. Snyder, J.G. Leesch, Methyl bromide recovery on activated carbon with repeated adsorption and electrothermal regeneration, Ind. Eng. Chem. Res. 40 (2001) 2925–2933, https://doi.org/10.1021/ie000395v.

[47] H.-J. Belt, M. Pittroff, M. Rieland, T. Schwarze, Method for recovering and/or separating sulfur oxyfluorides from gas mixtures, US6706090B2, 2004. https://patents.google.com/patent/US6706090B2/en (accessed May 28, 2020).

[48] S.A. Bouyoucos, R.G. Melcher, J.R. Vaccaro, Collection and determination of sulfuryl fluoride in air by ion chromatography, Am. Ind. Hyg. Assoc. J. 44 (1983) 57–61, https://doi.org/10.1080/15298668391404365.

[49] M. Harper, Novel sorbents for sampling organic vapours, Analyst 119 (1994) 65, https://doi.org/10.1039/an9941900065.

[50] Chao G., Hua Z., Zhu X., Elimination method of sulfuryl fluoride, CN104324704A, 2015. https://patents.google.com/patent/CN104324704A/en?oq=Cao%2c+G.;+Hua%2c+Z.;+Zhu%2c+X.;+Xiao%2c+D.;+Zheng%2c+J.;+Liu%2c+Z.;+Liu%2c+J.;+Sun%2c+B.+Method+for+Removing+Sulfuryl+Fluoride+Using+Porous+Micropheres.+CN104324704A%2c+2015 (accessed July 6, 2020).

[51] S. Pourebrahimi, A. De Visscher, G.H. Peslherbe, DFT investigation of Pt-doped CTF-1 covalent triazine frameworks for adsorption and sensing of SF6 decomposition products, Surf. Interfaces 49 (2024) 104404, https://doi.org/10.1016/j.surfin.2024.104404.

[52] UOP LLC., HiSiv 3000 Adsorbent (Technical Datasheet), (2006). www.uop.com (accessed January 14, 2021)

[53] Aqua Air Adsorbens GmbH, Air CC 816 (Technical Datasheet), (2008). https://www.aqua-air-adsorbens.de/

[54] CarboTech AC GmbH, CarboTech DGF 3 Super (Technical Datasheet), (2019). https://www.carbotech.de

[55] CarboTech AC GmbH, CarboTech D 47/3 Extra KC 10 (Technical Datasheet), (2019). https://www.carbotech.de

[56] K.-D. Henning, S. Schäfer, Impregnated activated carbon for environmental protection, Gas. Sep. Purif. 7 (1993) 235–240, https://doi.org/10.1016/0950-4214(93)80023-P.

[57] A. Möller, R. Eschrich, C. Reichenbach, J. Guderian, M. Lange, J. Möllmer, Dynamic and equilibrium-based investigations of CO2-removal from CH4-rich gas mixtures on microporous adsorbents, Adsorption 23 (2017) 197–209, https://doi.org/10.1007/s10450-016-9821-x.

[58] D.M. Ruthven, Principles of Adsorption and Adsorption Processes, Wiley, New York, 1984.

[59] J.U. Keller, R. Staudt, Gas Adsorption Equilibria: Experimental Methods and Adsorptive Isotherms, Springer, New York, 2005.
[60] H.-J. Bart, U. von Gemmingen, Adsorption, in: Wiley-VCH Verlag GmbH & Co. KGaA (Ed.), Ullmanns Encycl. Ind. Chem., Wiley-VCH Verlag GmbH & Co. KGaA, Weinheim, Germany, 2005: p. b03_09.pub2. https://doi.org/10.1002/14356007.b03_09.pub2.
[61] D. Bathen, M. Breitbach, Adsorptionstechnik, Springer Berlin Heidelberg, Berlin, Heidelberg, 2001, https://doi.org/10.1007/978-3-642-18235-8.
[62] S. Sharma, S.R.G. Balestra, R. Baur, U. Agarwal, E. Zuidema, M.S. Rigutto, S. Calero, T.J.H. Vlugt, D. Dubbeldam, RUPTURA: simulation code for breakthrough, ideal adsorption solution theory computations, and fitting of isotherm models, Mol. Simul. 49 (2023) 893–953, https://doi.org/10.1080/08927022.2023.2202757.
[63] E. Glueckauf, Theory of chromatography. Part 10.—Formulæ for diffusion into spheres and their application to chromatography, Trans. Faraday Soc. 51 (1955) 1540–1551, https://doi.org/10.1039/TF9555101540.
[64] W. Kast, Adsorption aus der gasphase: ingenieurwissenschaftliche grundlagen und technische verfahren, VCH, Weinheim, 1988.
[65] VDI 3674 - Abgasreinigung durch Adsorption - Prozessgas- und Abgasreinigung, n. d. https://www.vdi.de/richtlinien/details/vdi-3674-abgasreinigung-durch-adsorption-prozessgas-und-abgasreinigung (accessed October 2, 2020)
[66] M. Králik, Adsorption, chemisorption, and catalysis, Chem. Pap. 68 (2014), https://doi.org/10.2478/s11696-014-0624-9.
[67] M. Thommes, K. Kaneko, A.V. Neimark, J.P. Olivier, F. Rodriguez-Reinoso, J. Rouquerol, K.S.W. Sing, Physisorption of gases, with special reference to the evaluation of surface area and pore size distribution (IUPAC Technical Report), Pure Appl. Chem. 87 (2015) 1051–1069, https://doi.org/10.1515/pac-2014-1117.
[68] W. Kast, Adsorption aus der gasphase — grundlagen und verfahren, Chem. Ing. Tech. 53 (1981) 160–172, https://doi.org/10.1002/cite.330530304.
[69] smartGAs, FLOWEVO Infrared gas Sensor Sulfuryl Flouride SO2F2 4 Vol.-% smartGAS item number: F3–412406-05000, (2021). https://www.smartgas.eu/gase/so2f2-sensor (accessed August 23, 2025)
[70] M. Kraus, U. Trommler, F. Holzer, F.-D. Kopinke, U. Roland, Competing adsorption of toluene and water on various zeolites, Chem. Eng. J. 351 (2018) 356–363, https://doi.org/10.1016/j.cej.2018.06.128.
[71] J. Kärger, D.M. Ruthven, Diffusion in nanoporous materials: fundamental principles, insights and challenges, N. J. Chem. 40 (2016) 4027–4048, https://doi.org/10.1039/C5NJ02836A.
[72] Z. Bao, L. Yu, T. Dou, Y. Gong, Q. Zhang, Q. Ren, X. Lu, S. Deng, Adsorption equilibria of CO_2, CH_4, N_2, O_2, and ar on high silica zeolites, J. Chem. Eng. Data 56 (2011) 4017–4023, https://doi.org/10.1021/je200394p.
[73] J. Nastaj, T. Aleksandrzak, Adsorption isotherms of water, Propan-2-ol, and methylbenzene vapors on grade 03 silica gel, sorbonorit 4 activated carbon, and HiSiv 3000 zeolite, J. Chem. Eng. Data 58 (2013) 2629–2641, https://doi.org/10.1021/je400517c.
[74] I. Toreci, F.H. Tezel, Y. Yong, A. Sayari, Adsorption separation of methyl chloride from nitrogen using ZSM-5 and mesoporous SBA-15, Adsorpt. Sci. Technol. 24 (2006) 79–99, https://doi.org/10.1260/026361706778062577.
[75] J. Kärger, D.M. Ruthven, D.N. Theodorou, Diffusion in nanoporous materials: KAERGER:DIFFUSION 2V O-BK, Wiley-VCH Verlag GmbH & Co. KGaA, Weinheim, Germany, 2012, https://doi.org/10.1002/9783527651276.
[76] R.W. Broach, D.-Y. Jan, D.A. Lesch, S. Kulprathipanja, E. Roland, P. Kleinschmit, Zeolites. Ullmanns Encycl. Ind. Chem, American Cancer Society, 2012, https://doi.org/10.1002/14356007.a28_475.pub2.